Title

Refinement of a coarse-grained model of poly(2,6-dimethyl-1,4-phenylene ether) and its application to blends of PPE and PS

Journal

Molecular Simulation, 42(4)

ISSN

0892-7022

Authors

Wang, Huan
Shentu, Baoqing
Faller, Roland

Publication Date

2016-03-03

DOI

10.1080/08927022.2015.1047368

Peer reviewed

Refinement of a Coarse-Grained Model of Poly(2,6-dimethyl-1,4-phenylene ether) and its Application to blends of PPE and PS

Huan Wang[a,b], Baoqing Shentu*[b] and Roland Faller*[a],

[a] *Department of Chemical Engineering & Materials Science, University of California at Davis, One Shields Ave, Davis, California 95616, United States*

[b]*State Key Lab of Chemical Engineering, College of Chemical and biological Engineering, Zhejiang University, Hangzhou 310027, China*

**Corresponding authors. Email: rfaller@ucdavis.edu; shentu@zju.edu.cn.*

Abstract:

A coarse-grained (CG) molecular simulation model has been refined for poly (2,6-dimethyl-1,4-phenylene ether) (PPE). This was successfully validated against atomistic simulation and experimental data. Particularly, the glass transition temperature (T_g) of PPE was studied using both atomistic and CG models and compared favorably to experimental data. In addition, we used the CG model together with an existing Martini CG model of polystyrene (PS) to study the blending behavior of these two polymers. We solved the problem to mix the different potentials and molecular dynamics of high-molecular-weight blends of PPE/PS was performed in detail.

Keywords: Coarse-grained model, molecular dynamics simulation, poly(2,6-dimethyl-1,4-phenylene ether), polystyrene

1. Introduction

Molecular dynamics (MD) simulation has been extensively used to study physical and chemical properties of a wide variety of polymers [1-12]. However, conventional atomistic molecular dynamic simulations of high-molecular-weight polymer melts are subject to severe limitations of computational resources in both time and length scales. Coarse grained (CG) models provide a means to expand the utility of existing computational resources by allowing the exploration of far greater temporal and spatial scales than simulations in full atomistic detail. Basically, CG models group clusters of atoms into super-atoms, or beads, thus reducing the total number of interaction sites in the system. With this approach in mind, many groups have developed CG models using various approaches with numerous applications appearing in the literature over the past four decades [13-17]. But most CG models have focused on a few classical polymer types such as polystyrene (PS) [18-26]. Many other polymers like, e.g, poly (2,6-dimethyl-1,4-phenylene ether) (PPE) are largely ignored despite their importance.

A standard CG model for polymers, lipids and other molecules of biological interest is the MARTINI model [27-31], and this model has been extended to polymers like PS, [32,33] poly(ethylene glycol) [34], poly(ethylene oxide) and dendrimers [35] etc. Benzene rings are modelled by three beads in the MARTINI approach. But the benzene rings in PPE chains are connected in their para-position with each other, therefore (Scheme 1), a three-bead ring is not appropriate. A CG model for phenyl-based molecules has been developed by DeVane *et al*, [36] which

provides an alternative strategy for the construction of a CG model for PPE. However, PPE is not usually applied in its pure form, and PPE/PS is the most common PPE based blend in industry [37-43]. Thus, making this CG model suitable for the study of blends is necessary.

In this contribution, we present the refinement of a CG model for PPE and its application of modeling bulk PPE melts and PPE/PS blends by combining this model with a Martini based CG model for PS.

2. Models and Methods

2.1 Models

The Construction of Coarse-Grained Model for PPE. The CG model of PPE presented here is developed based on previous work by DeVane et al. [36]. The model uses three types of coarse-grained beads for PPE, and each repeating unit is represented by four beads, leading to a mapping ratio of 4 CG sites to 18 atoms. Scheme 1 shows the atomistic description of PPE is mapped onto the coarse-grained model.

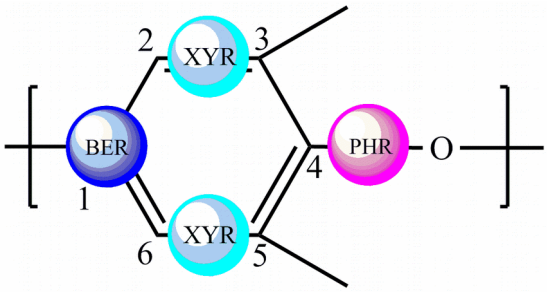

Scheme 1 The CG mapping of a PPE unit

The PPE CG model is composed of two XYR beads, a BER bead and a PHR bead. Here, a BER bead represents one of the four equivalent sites of a benzene ring with no side groups, XYR beads represent a BER bead with a methyl group attached,

and a PHR bead represents a BER bead with an oxygen or a hydroxyl group attached. The intramolecular potential was parametrized to reproduce the bond distances and angles taken from a geometry-optimized structure. The center of mass of C1, a quarter of C2, and a quarter of C6 as well as the hydrogens attached are assigned to BER; the center of mass of C4, a quarter of C3, a quarter of C5 and the oxygen is subsumed into PHR. The center of mass of the methyl group attach to C3 and three quarters of C2 and C3 is the location of one XYR. Similarly the location of the other XYR could be located. Bonds between CG beads are modeled via harmonic potentials with an equilibrium bond length r_0 and a force constant k_b. Equivalently we have harmonic angles with □□$_0$and k_a. A dihedral angle maintains a planar ring geometry (Eq.1).

$$v(\theta)_{dihedral} = k_d[1 + \cos(n\theta - d)] \quad \text{Eq.1}$$

Here, k_d is the force constant, n determines the periodicity, d is the equilibrium dihedral angle. Nonbonded interactions between noncharged beads are described by 9-6 potentials and Lorentz-Berthelot like combining rules generate the cross interactions of different CG sites (Eq 2 & 3).

$$v(r)_{9\text{-}6} = 4\varepsilon_{9\text{-}6}\left(\frac{\sigma_{9\text{-}6}^{9}}{r^{9}} - \frac{\sigma_{9\text{-}6}^{6}}{r^{6}}\right) \quad \text{Eq.2}$$

$$\sigma_{ab} = \frac{\sigma_{aa} + \sigma_{bb}}{2} \quad \varepsilon_{ab} = \sqrt{\varepsilon_{aa}\varepsilon_{bb}} \quad \text{Eq.3}$$

Here, □$_{aa}$ and □$_{aa}$ represent the self-interaction value,□□□$_{ab}$ and □$_{ab}$ represent those for the cross interaction. All parameters are listed in Tables 1-4.

Parameters for the PHR-XYR bond, XYR-PHR-XYR angle, PHR-XYR-BER

angle, BER-PHR-XYR angle, BER-XYR-PHR-BER dihedral, XYR-PHR-BER-XYR dihedral, and PHR-BER-XYR-PHR dihedral are calculated according to the structural information provided by the atomistic force field PCFF [44-54], since they are not available in DeVane's work. Considering the difference between the PPE polymer and its DMP monomer, we make several adjustments to other parameters in order to make the parameters suitable for PPE in this study, especially to the PHR bead, because most of the PHR beads here represent a BER bead with an ether oxygen rather than a hydroxyl oxygen. Additionally, the densities of both DMP and PPE (degree of polymerization DP=20) are used as the target to adjust the set of non-bonded parameters.

Table 1 Bond parameters

types	k_b (kcal/mol/Å^2)	r_0(Å)
BER-XYR	40.0	2.700
PHR-XYR	40.0	3.100
BER-PHR	40.0	1.800

Table 2 Angle Parameters

types	k_a (kcal/mol/radian^2)	□□(degree)
XYR-BER-XYR	30.0	112.317
XYR-PHR-XYR	30.0	91.357
PHR-XYR-BER	30.0	78.163
BER-PHR-XYR	30.0	117.000
XYR-BER-PHR	30.0	111.000

Table 3 Dihedral Parameters (Eq.1)

types	k_d (kcal/mol)	n	d (degree)	weighting factor
BER-XYR-PHR-XYR	60.0	1	180.0	0
BER-XYR-PHR-BER	30.0	1	60.0	0
XYR-PHR-BER-XYR	30.0	1	120.0	0
PHR-BER-XYR-PHR	30.0	1	60.0	0

Table 4 Nonbonded parameters for Eq. 2 and 3

types	□	□
BER	0.295	3.850
PHR	0.928	3.550
XYR	0.54	4.050

The combination of CG models of PPE and PS. The CG model of PS employed here is the Martini based model developed by Rossi et al. [32,33]. In contrast to the 9-6 model for PPE, a standard Lennard Jones 12-6 potential function (Eq.4) is used for PS and shifted as is customary for Martini. In order to solve the problem of combining two different non-bonded potential forms, we tried mixing the potentials by arithmetic and geometric means, and compared the results to the atomistic data. An arithmetic average was chosen to be the mixing potential (Eq.5 and Table 5). Clearly such a mixing has no direct physical meaning but it can only be justified by testing.

$$v(r)_{12\text{-}6} = 4\varepsilon_{12\text{-}6}\left(\frac{\sigma_{12\text{-}6}^{12}}{r^{12}} - \frac{\sigma_{12\text{-}6}^{6}}{r^{6}}\right) \qquad \text{Eq.4}$$

$$v(r)_{mix} = 1/2\left[4\varepsilon_{9\text{-}6}\left(\frac{\sigma_{9\text{-}6}^{9}}{r^{9}} - \frac{\sigma_{9\text{-}6}^{6}}{r^{6}}\right) + 4\varepsilon_{12\text{-}6}\left(\frac{\sigma_{12\text{-}6}^{12}}{r^{12}} - \frac{\sigma_{12\text{-}6}^{6}}{r^{6}}\right)\right] \qquad \text{Eq.5}$$

Table 5 Nonbonded mixing parameters for Eq.5

Types	□	□
BER	1.18	4.235
PHR	3.721	3.905
XYR	2.16	4.455
B	2.5	4.730
R	2.4	4.510

2.2 Simulation Details

All simulations were carried out using the LAMMPS code developed by Sandia National Laboratory [55] and analysis was performed using VMD [56]. The polymer consistent force field (PCFF) [44-54] was employed throughout the atomistic

simulations. The simulations employ periodic boundary condition in all directions and all PS chains in the atomistic simulations are isotactic. For setting up pure PPE, we first put one chain in a box, for PPE/PS blends, we put one chain for each polymer in a box. And then we replicated the whole box as many times as needed and made sure that the final box is cubic. Constant temperature and constant pressure (p=1 atm) molecular dynamics simulations were performed using the Nose-Hoover thermostat and barostat [44] after minimization to equilibrate the system for 100 ns, and the equilibrations of all systems were monitored by density as a function of time. The atomistic simulations used a timestep of 1fs, and CG simulations employed a timestep of 10 fs, and all PPE/PS blends were 50:50 (by mol). More details about the simulations of different systems are listed in Table 6.

Table 6 Details of atomistic and CG simulations performed

□	□	DP	n_{PPE}	n_{PS}
Atomistic	pure PPE	5	36	—
		10	36	—
		20	36	—
		30	36	—
	PPE/PS	10	27	27
		20	27	27
CG	pure PPE	5	36	—
		10	36	—
		20	36	—
		30	36	—
		50	36	—
		80	36	—
		100	36	—
	PPE/PS	10	64	64
		20	64	64
		50	40	40

		80	40	40

DP, n_{PPE} and n_{PS} are the polymerization degrees, the number of PPE chains and the number of PS chains.

After the equilibration of the systems, glass transition temperatures (T_g) of PPE with different polymerization degrees (DP) were obtained by performing cooling NPT simulations from 800 K to 1 K in 20 ns. Radii of gyration were calculated every 20000 steps over 10000000 steps. Mean squared displacements were also calculated with a running time average (Nevery=20, Nrepeat=100 and Nfreq=20000) after the equilibration.

3. Results and Discussion

3.1 Coarse-Grained model of PPE

The density of the monomer 2,6-dimethylphenol (DMP) is calculated at 323.15K which is slightly above the melting point (318.15-320.15K) to make sure that the model is appropriate for this system. The density of DMP at 323.15 K in the liquid state is measured to be 0.97 g/cm^3 using Dilatometer DIL402C produced by Netzsch, Germany. in experiment, and the densities calculated here by AA and CG MD are 0.95g/cm^3 and 0.98g/cm^3 (the relative errors are estimated to be -2.06% and +1.03%), respectively, showing these two models are reliable for this property. The radial distribution functions (RDFs) from bulk PPE simulations are calculated to test the structural properties of the CG model against atomistic data. As shown in Scheme 2, we use the same position (red circle) in each unit of polymer chain to calculate the RDFs from AA MD and CG MD. The shapes of CG RDF line (dashed line) agree reasonably well with that of AA simulations (solid line) in Figure 1. It is worth noting

that this is not a structurally coarse-grained model such that perfect agreement cannot be expected. The agreement is essentially independent of chain length. The main discrepancy is in the area around 7 Å where the atomistic data predicts a deeper dip, i.e. a locally more pronounced structure.

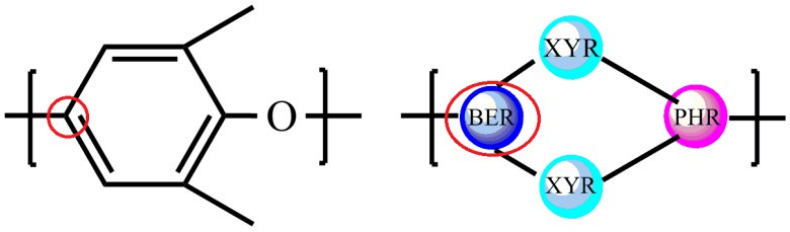

Scheme 2

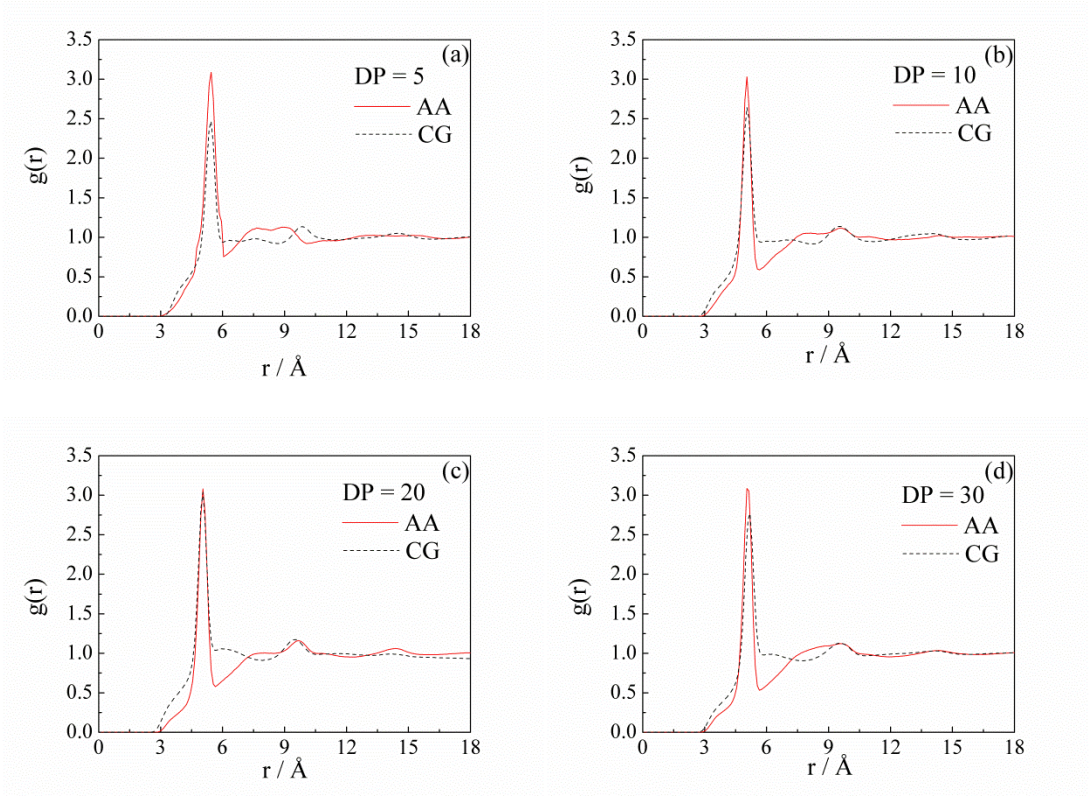

Figure 1 Radial distribution functions in atomistic and coarse-grained representation for different degrees of polymerization

The structure factors (S(k)) of coarse-grained simulations with different DPs are calculated [57] and they are shown in Figure 2 in comparison to the atomistic ones.

The S(k) calculated from both type of simulations are in good agreement. They both show a clear peak at 1.5 nm and some other smaller peaks around 2~10 nm.

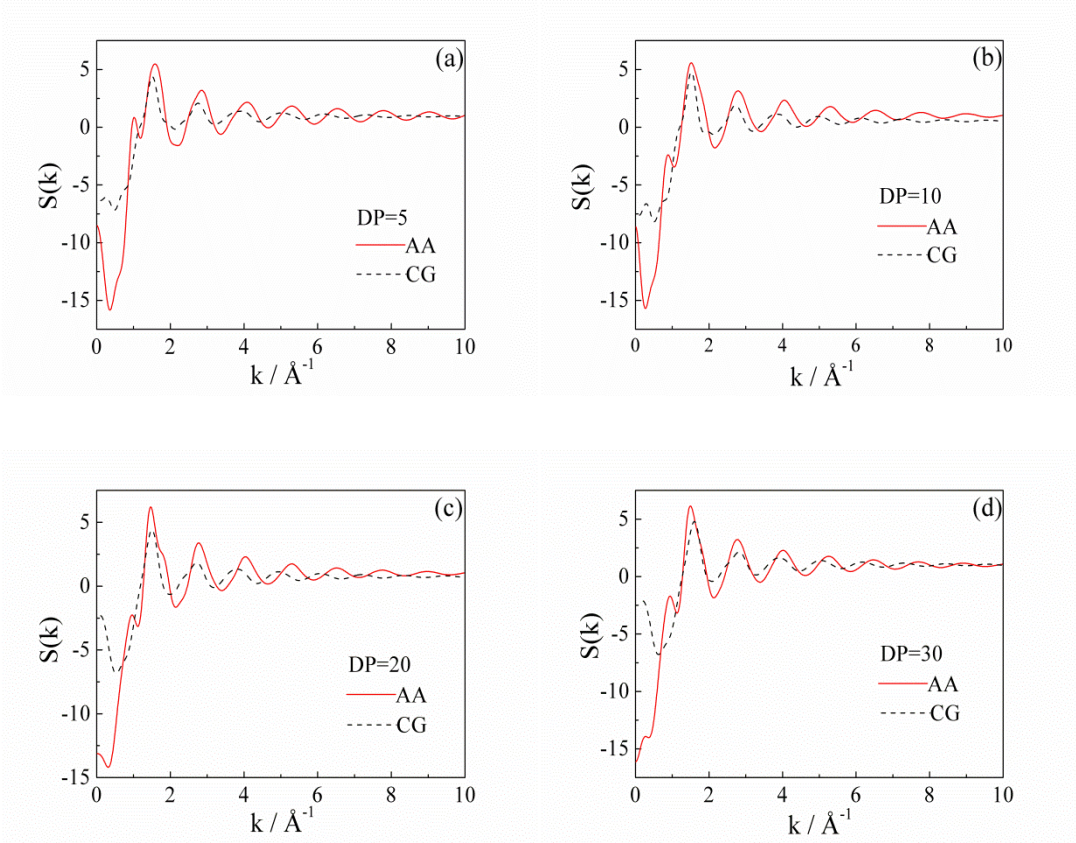

Figure 2 Structure factors of atomistic and coarse-grained models for different degrees of polymerization

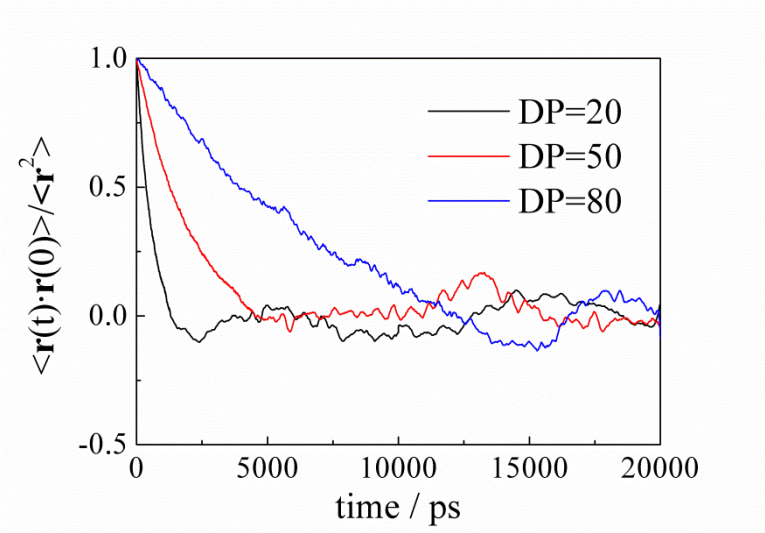

Figure 3 The end-to-end autocorrelation function for coarse-grained simulations with different degrees of polymerization

Furthermore, Figure 3 presents the decay of the autocorrelation function for the end-to-end vector [58] with chain lengths ranging from 20 to 80 for the coarse-grained simulations of PPE. The rates of $\langle \mathbf{r}(t) \cdot \mathbf{r}(0) \rangle / \langle \mathbf{r}^2 \rangle$ approaching zero measures how long the chains need to "forget" their initial conformations. As shown in the figure, the relaxation time rise with increasing chain length, and it takes about 1.3 ns for chains with DP=20 to reach zero, for the chains with DP=50 this time increases to approximately 4.5 ns, and it can take as long as 12 ns for the chains with DP=80 to relax, thus a equilibration time of 100 ns is enough for the systems to be prepared for the subsequent simulations.

Table 7 Radii of gyration for PPEs with different DP at 540 K

DP	R_g/Atomistic(Å)	R_g/CG(Å)
5	6.30	6.80
10	10.7	11.26
20	11.98	12.16
30	15.20	14.70
50	—	17.23
80	—	27.03
100	—	32.35

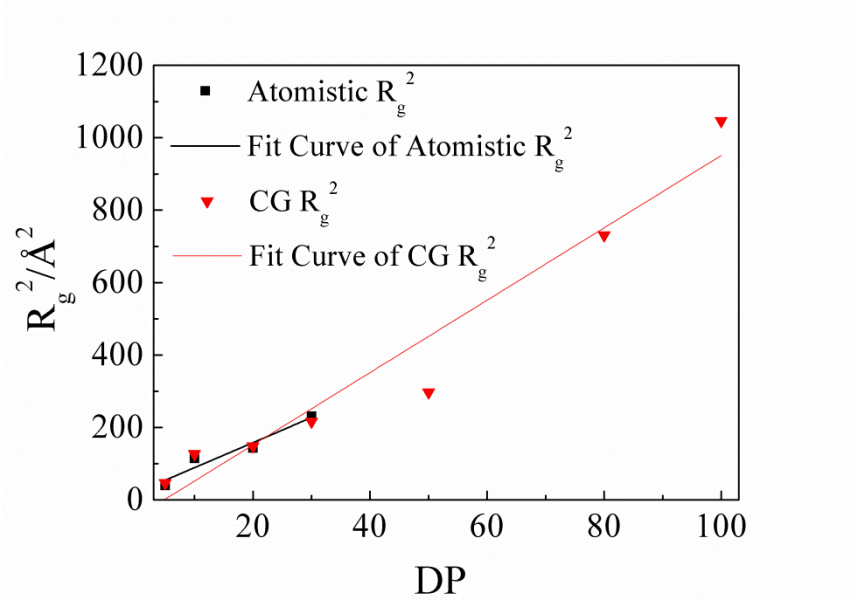

Figure 4 R_g^2 versus DP for atomistic and CG simulations

The glass transition is one of the most important properties of polymers for theoretical and practical reasons, it is usually studied through isobaric conditions [59], during which the volume varies in accordance with the temperature change. As the temperature increases the change in free volume of a polymer is small below the glass transition temperature (T_g) but the rate of change increases abruptly at T_g. Thus T_g can be determined as the temperature marking the discontinuity in slope of the plots of V-T data for both atomistic and CG models here, and the results are compared to experimental data in Table 8.

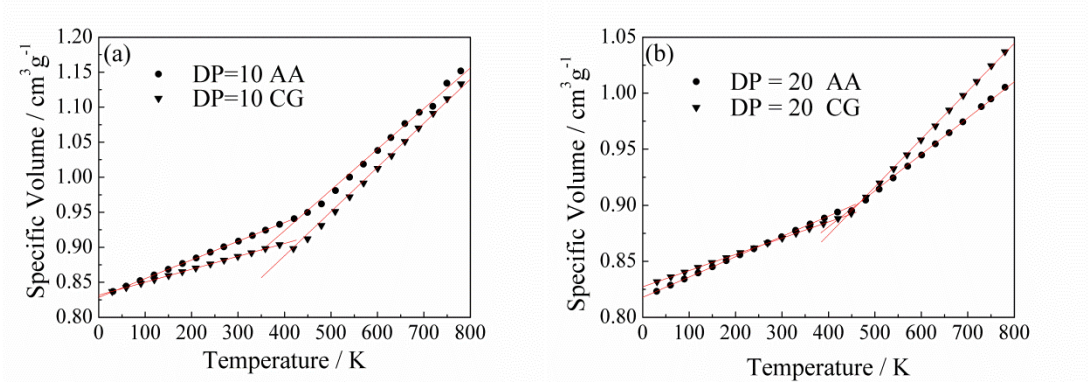

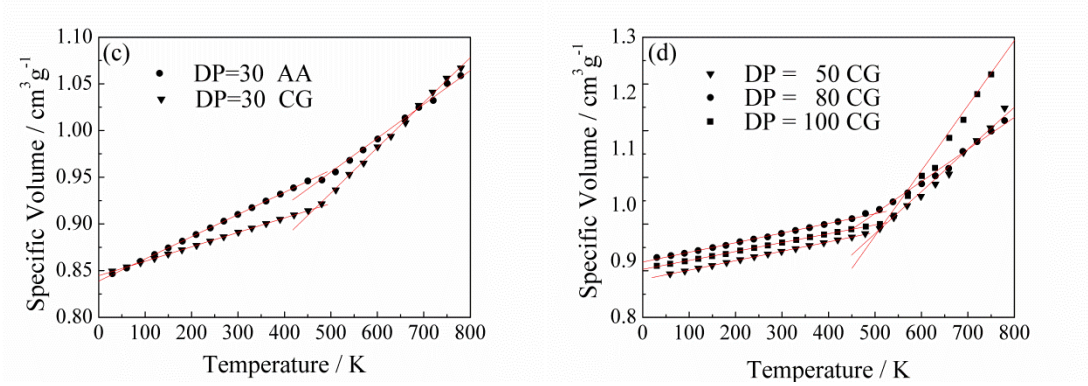

Figure 5 Specific volume in NPT simulations versus temperature for both AA and CG models of PPE with different DPs.

As shown in Table 7, the radii of gyration (R_g) at 540K for polymers with DP from 5 to 30 are calculated by both atomistic and CG MD, showing good agreement. In addition, R_g of PPE with DP=50, 80 and 100 are also calculated. It is obvious that R_g of PPE increases with the increasing of DP and R_g can be used to evaluate the size of the molecule. In addition, R_g^2 versus DP are plotted in Figure 4, and R_g^2 are approximately linear with DP for both atomistic and CG simulations indicating a random walk structure in the melt.

Table 8 Glass transition temperatures of PPE with different DPs

DP	Atomistic T_g /K	CG T_g /K	Experimental T_g /K [60,61]
10	437	440	405
20	467	440	437
30	517	465	457
50	—	504	470
80	—	499	478
100	—	522	480

It is clear from Figure 5 and Table 8 that the T_g from the CG model corresponds well with atomistic model during the cooling process. Most T_g are about 30-40 degrees higher than experimental data, [60,61] which is reasonable as the cooling rate

in MD simulation is much faster than in experiment, and in simulations, all polymers have exactly the same molecular weight. Simulations for high-molecular-weight PPEs are also run using CG model and T_g are calculated. T_g of PPE with DP=50, 80 and 100 are shown in Figure 3 and Table 8. Again the calculated T_g are all about 20~40 degrees higher than experimental values. All this illustrates that the CG model is appropriate to study PPE.

3.2 The Combination of CG Models for PPE and PS

Table 9 Densities for blending system with different DPs

DP	10	20	50	80
Atomistic □□(g/cm^{-3})	0.99	0.98		
CG□□ (g/cm^{-3})	0.98	0.96	0.90	0.90

Our main interest in parameterizing a CG model for PPE is to provide accurate dynamic information over longer times or for larger systems than is possible using atomistic simulations. We are also interested in the performance of the CG model for PPE when it is blended with another polymer. To evaluate this issue, we combine the CG model for PPE constructed above with the Martini PS model developed by Rossi et al. [32,33]. In order to make this combination work for a PPE/PS blend, we needed to develop mixing rules as described in Section 2.1. The densities of PPE/PS blends with different DPs for both atomistic and CG simulations are listed in Table 9. The results of RDFs for the atoms and beads shown in Scheme 3 of PPE/PS blend are presented in Figure 6. We compared the CG model to the atomistic one at DP=10. The RDF curves of the CG are reasonably close to the atomistic data considering again that the model was not structurally coarse-grained. The main different is that the atomistic double peak in Figure 6 (c) collapses into a broad single peak in the CG

model. Furthermore, we increase the molecular weight of polymers (Fig. 6 (d)) using the CG model, no phase separation is observed, meaning that all of the systems are miscible and the blend structure is only weakly dependent on molecular weight.

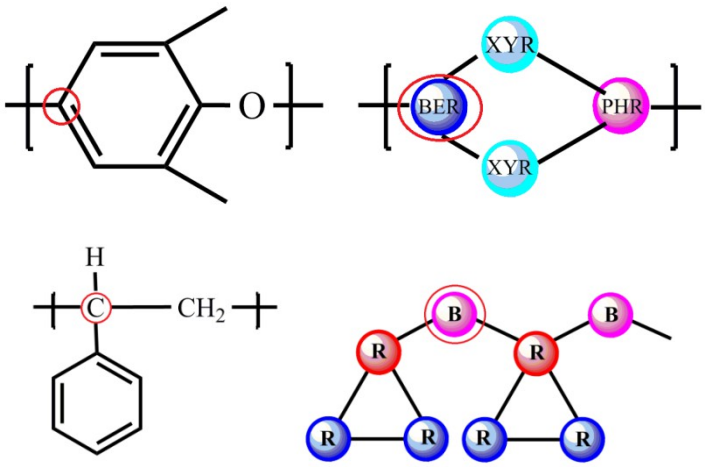

Scheme 3

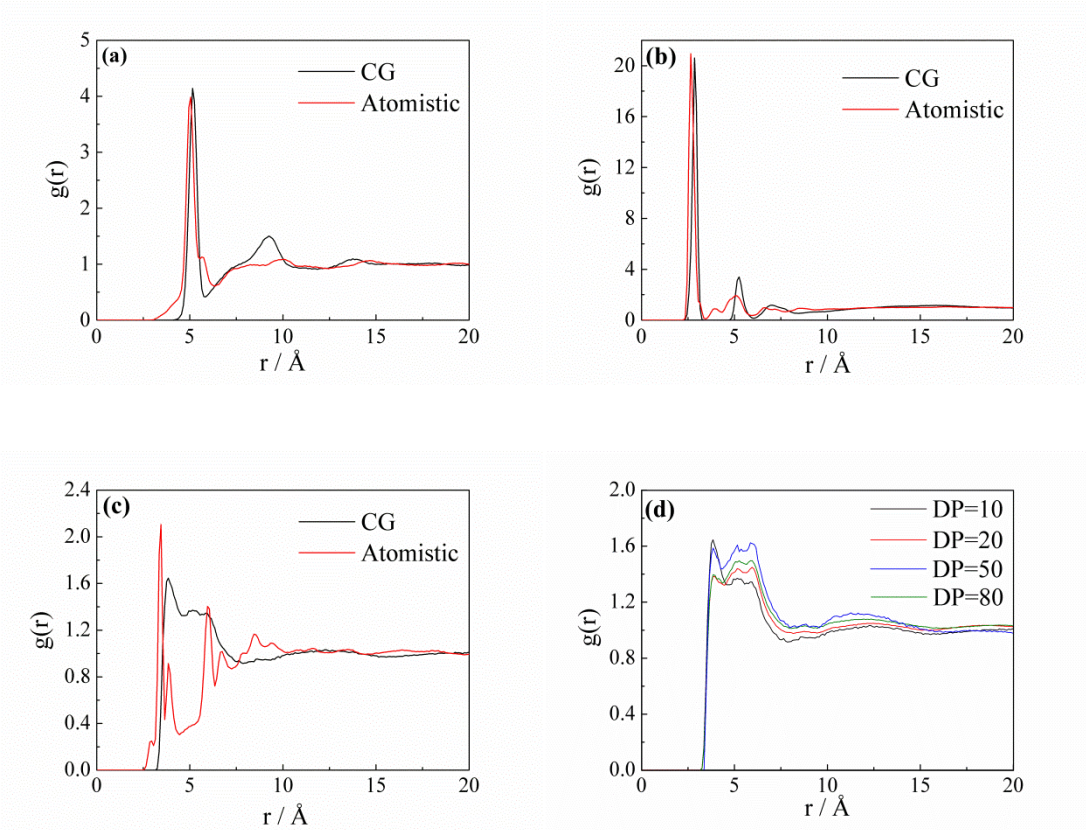

Figure 6 (a) RDF of benzene carbon and BER in PPE (DP=10) (b) RDF of C and

B in PS (DP=10) (c) RDF of PPE and PS (DP=10) (d) RDF of PPE and PS with different molecular weights for CG model

We estimate the sizes of the molecules by the radii of gyration (R_g), and the average R_g of PPE and PS for both atomistic and CG simulations are listed in Table 10 where we see that the CG simulation results agree well with atomistic simulation.

Table 10 Radii of gyration for PPE/PSs with different DP at 540 K/ Å

DP	R_g/AA(Å)		R_g/CG(Å)	
	PPE	PS	PPE	PS
10	11.4	6.52	11.6	6.7
20	11.98	10.03	12.9	10.4
50			17.4	14
80			34	23.6

We finally employ mean squared displacement (MSD) analysis to characterize the motion and to determine the mobility of central monomers of polymer chains. It can be observed from Figure 7 that the central monomers of PS move much faster than the ones of PPE chains. On the other hand, the mobility of central monomers first slightly increases with increasing molecular weight and then rapidly decreases. It can be explained that the flexibility of chains increases when DP increases (transitioning from oligomers to polymers), but when the molecular weight is large enough, the mobility of whole chain decreases rapidly, then the mobility of the central monomer decreases.

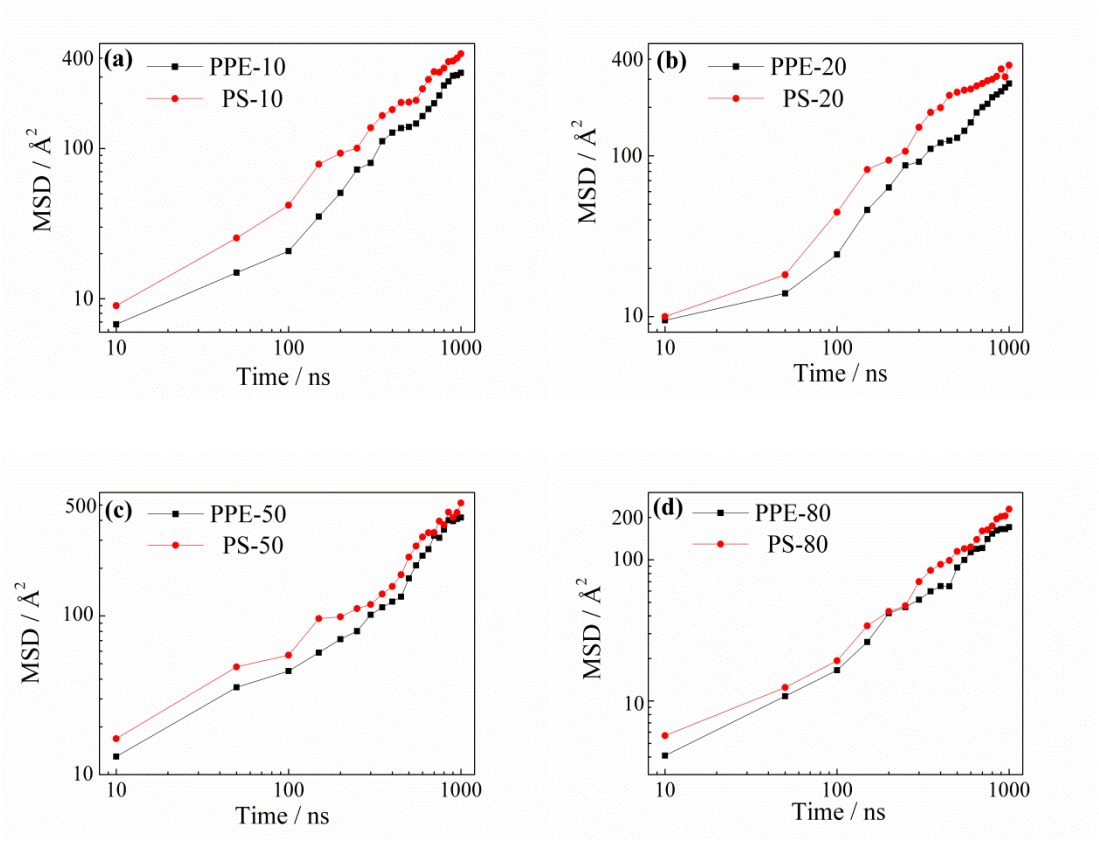

Figure 7 MSD of central monomers in PPE and PS with different polymerization degrees in the CG model

4. Conclusions

We construct a coarse-grained model for PPE based on previous work and evaluate this model by comparing the simulation results to the atomistic model and experimental data. In addition, we combine this newly developed CG model with another CG model for PS. This work has demonstrated the ability of this potential to model systems at the CG level with sufficient accuracy to predict the properties of PPE and its blends. The dynamics in the blend show that PPE is clearly the more mobile species.

Atomistic and CG simulations are in general in good agreement for the short

chains where atomistic simulations are possible. Thus, we can expect that the larger CG simulations of high molecular weight blends are also truthful models for the structure. The glass transition of PPE is predicted to within about 40 K which is very good agreement keeping in mind that the cooling rate is way too fast compared to experiments.

Acknowledgements. This study was supported by China Scholarship Council.

References

1. W. Paul, G. D. Smith, D. Y. Yoon. *Macromolecules,* **1997**, *30*, 7772.
2. W. Paul, G. D. Smith, D. Y. Yoon, B. Farago, S. Rathgeber, A. Zirkel, L. Willner, D. Richter. *Phys. Rev. Lett.,* **1998**, *80*, 2346.
3. M. Mondello, G. S. Grest. *J. Chem. Phys.*, **1997**, *106*, 9327.
4. J. D. Moore, S. T. Cui, H. D. Cochran, P. T. Cummings. *J. Non-Newtonian Fluid Mech.,* **2000**, *93*, 83.
5. V. Harmandaris, V. G. Mavrantzas, D. N. Theodorou. *Macromolecules*, **2000**, *33*, 8062.
6. J. T. Padding, W. J. Briels. *J. Chem. Phys.*, **2001**, *114*, 8685.
7. K. Hur, R. G. Winkler, D. Y. Yoon. *Macromolecules*, **2006**, *39*, 3975.
8. M. Bulacu, E. van der Giessen. *Rhys. Rev. E*, **2007**, *76*, 11807.
9. M. Lang. *Macromolecules*, **2013**, *46*, 9782.
10. J. Koski, H. Chao, R. A. Riggleman. *J. Chem. Phys*., **2013**, *139*, 244911.
11. Y. Feng, N. Ning, Q. Zhao, J. Liu, L. Zhang, M. Tian, J. Mi. *Soft Matter*, **2014**, *10*, 8236.
12. O. G. Kravchenko, C. Li, A. Strachan, S. G. Kravchenko, R. B. Pipes.

Composites: Part A, **2014**, *66*, 35.

13. J. J. de Pablo. *Annu. Rev. Phys. Chem*., **2011**, *62*, 555.
14. A. Milchev. *J. Phys. Condens. Matter*, **2011**, *23*, 103101.
15. J. T. Padding, W. J. Briels. *J. Phys. Condens. Matter*, **2011**, *23*, 2333101.
16. Y. Li, B. C. Abberton, M. Kroger, W. K. Liu. *Polymers*, **2013**, *5*, 751.
17. E. Brini, E. A. Algaer, P. Ganguly, C. Li, F. Rodriquez-Ropero, N. F. A. van der Vegt. *Soft Matter*, **2013**, *9*, 2108.
18. W. Tschop, K. Kremer, J. Batoulis, T. Burger, O. Hahn. *Acta Polym.*, **1998**, *49*, 61.
19. G. Milano, Muller-Plathe. *J. Phys. Chem. B.*, **2005**, *109*, 18609.
20. P. Carbone, H. A. K. Varzaneh, X. Chen, F. Muller-Plathe. *J. Chem. Phys.*, **2008**, *128*, 064904.
21. Q. Sun, R. Faller. *Comput. Chem. Eng*., **2005**, *29*, 2380.
22. D. Fritz, V. A. Harmandaris, K. Kremer, N. F. A. van der Vegt. *Macromolecules*, **2009**, *42*, 7579.
23. A. Ghanbari, M. Rahimi, J. Dehghany. *J. Phys. Chem. C.*, **2013**, *117*, 25069.
24. C. Wu. *Macromolecules*, **2013**, *46*, 5751.
25. C. Wu. *J. Mol. Model.*, **2014**, *20*, 2377.
26. L. Liu, W. K. den Otter, W. J. Briels. *Soft Matter*, **2014**, *10*, 7874.
27. S. J. Marrink, A. H. de Vries, A.E. Mark. *J. Phys. Chem. B.*, **2004**, *108*, 750.
28. S. J. Marrink, H. J. Risselada, S. Yefinov, D.P. Tieleman, A.H. de Vries. *J. Phys. Chem. B.*, **2007**, *111*, 7812.
29. L. Monticelli, S. K. Kandasamy, X. Periole, R.G. Larson, D.P. Tieleman, S. J.

Marrink. *J. Chem. Theory Comput.*, **2008**, *4*, 819.

30. A. Catte, T. Vuorela, P. Niemela, T. Murtola, J. P. Segrest, S. J. Marrink, M. Karttunen, I. Vattulainen. *Biophys. J.*, **2008**, *94*, 983.

31. T. Vuorela, A. Catte, P. X. Niemela, A. Hall, M. T. Hyvonen, S. J. Marrink, M. Karttunen, I. Vattulainen. *PLoS Comput. Biol.*, **2010**, *6*, e1000964.

32. G. Rossi, L. Monticelli, S. R. Puisto, I. Vattulainen, T. Ala-Nissila. *Soft Matter*, **2011**, *20*, 305.

33. G. Rossi, I. G. Elliott, T. Ala-Nissila, R. Faller. *Macromolecules*, **2012**, *45*, 563.

34. H. Lee, A. H. de Vries, S. J. Marrink, R. W. Pastor. *J. Phys. Chem. B.*, **2009**, *113*, 13198.

35. H. Lee, R.G. Larson. *J. Phys. Chem. B.*, **2008**, *112*, 7778.

36. R. DeVane, M. L. Klein, C. Chiu, S. O. Nielsen, W. Shinoda, P. B. Moore. *J. Phys. Chem. B.*, **2010**, *114*, 6386.

37. A. S. Hay, *J. Polym. Sci., Part A: Polym. Chem.*, **1998**, *36*, 505.

38. G. D. Merfeld, G. W. Yeager, H. S. Chao, N. Singh. *Polymer*, **2003**, *44*, 4981.

39. R. T. Tol, V. B. F. Mathot, G. Groeninckx. *Polymer*, **2005**, *46*, 369.

40. H. Eklind, S. Schantz, F. H. J. Maurer, P. Jannasch, B. Wesslen. *Macromolecules*, **1996**, *29*, 984.

41. J. Y. Cavaille, S. Etienne, J. Perez, L. Monnerie, G. P. Johari. *Polymer*, **1986**, *27*, 549.

42. J. Stoelting, F. E. Karasz, W. Macknight. *J .Polym. Eng. Sci.*, **1970**, *10*, 133.

43. H. R. Brown, K. Char, V. R. Deline, P. F. Green. *Macromolecules*, **1993**, *26*, 4155.

44. M. J. Hwang, T. P. Stockfisch, A. T. Hagler. *J. Am. Chem. Soc.*, **1994**, *116*, 2515.

45. J. R. Maple, M. J. Hwang, T. P. Stockfisch, U. Dinur, M. Waldman, C. S. Ewig, A. T. Hagler. *J. Comput. Chem.*, **1994**, *15*, 162.

46. J. R. Maple, M. J. Hwang, T. P. Stockfisch, A. T. Hagler. *Isr. J. Chem.*, **1994**, *34*, 195.

47. Z. W. Peng, C. S. Ewig, M. J. Hwang, M. Waldman, A. T. Hagler. *J. Phys. Chem. A.*, **1997**, *101*, 7243.

48. H. Sun. *J. comput. Chem.*, **1994**, *15*, 752.

49. H. Sun, S. J. Mumby, J. R. Maple, A. T. Hagler. *J. Am. Chem. Soc.*, **1994**, *116*, 2978.

50. H. Sun. *Macromolecules*, **1995**, *28*, 701.

51. H. Sun. *Macromolecules*, **1994**, *26*, 5924.

52. H. Sun, S. J. Mumby. J. R. Maple, A. T. Hagler. *J. Phys. Chem.*, **1995**, *99*, 5873.

53. H. Sun. *J. Phys. Chem. B.*, **1998**, *102*, 7338.

54. PCFF is available in LAMMPS package.

55. S. J. Plimpton, Large-scale atomic/molecular massively parallel simulator. Sandia National Laboratories, **2007**.

56. W. Humphrey, A. Dalke, K. Schulten. *J. Mol. Graphics*, **1996**, *14*, 33.

57. C. Fan, T. Cagin, Z. Chen, K. Smith. *Macromolecules*, **1994**, *27*, 2383.

58. V. A. Harmandaris, V. G. Mavrantzas, D. N. Theodorou. *Macromolecules*, **1998**, *31*, 7934.

59. K. Yu, Z. Li, J. Sun. *Macromol. Theory Simul.*, **2001**, *10*, 624.

60. T. G. Fox, P. J. Flory. *J. Am. Chem. Soc.*, **1948**, *70*, 2384.

61. T. G. Fox, P. J. Flory. *J. Appl. Phys.*, **1950**, *21*, 581.